Author Manuscript

Authors: Shunichi Fukuzumi, Prof.; Jieun Jung; Yusuke Yamada; Takahiko Kojima;
Wonwoo Nam

Homogeneous and Heterogeneous Photocatalytic Oxidation of Water by Persulfate

Shunichi Fukuzumi,*[a, b, c] Jieun Jung,[a] Yusuke Yamada,*[d] Takahiko Kojima,*[e] and Wonwoo Nam*[a]
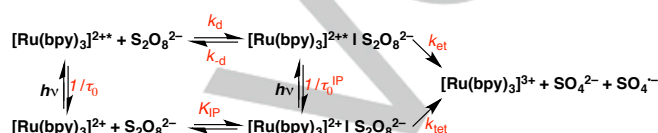
$4[SO_4]^{2-}$ $4[Ru(bpy)]^{3+}$ $2H_2O$

$h\nu$ WOC

$2[S_2O_8]^{2-}$ $4[Ru(bpy)]^{2+}$ $O_2 + 4H^+$

Water Oxidation Catalysts

polyoxometalates   metal complexes   coordination polymers
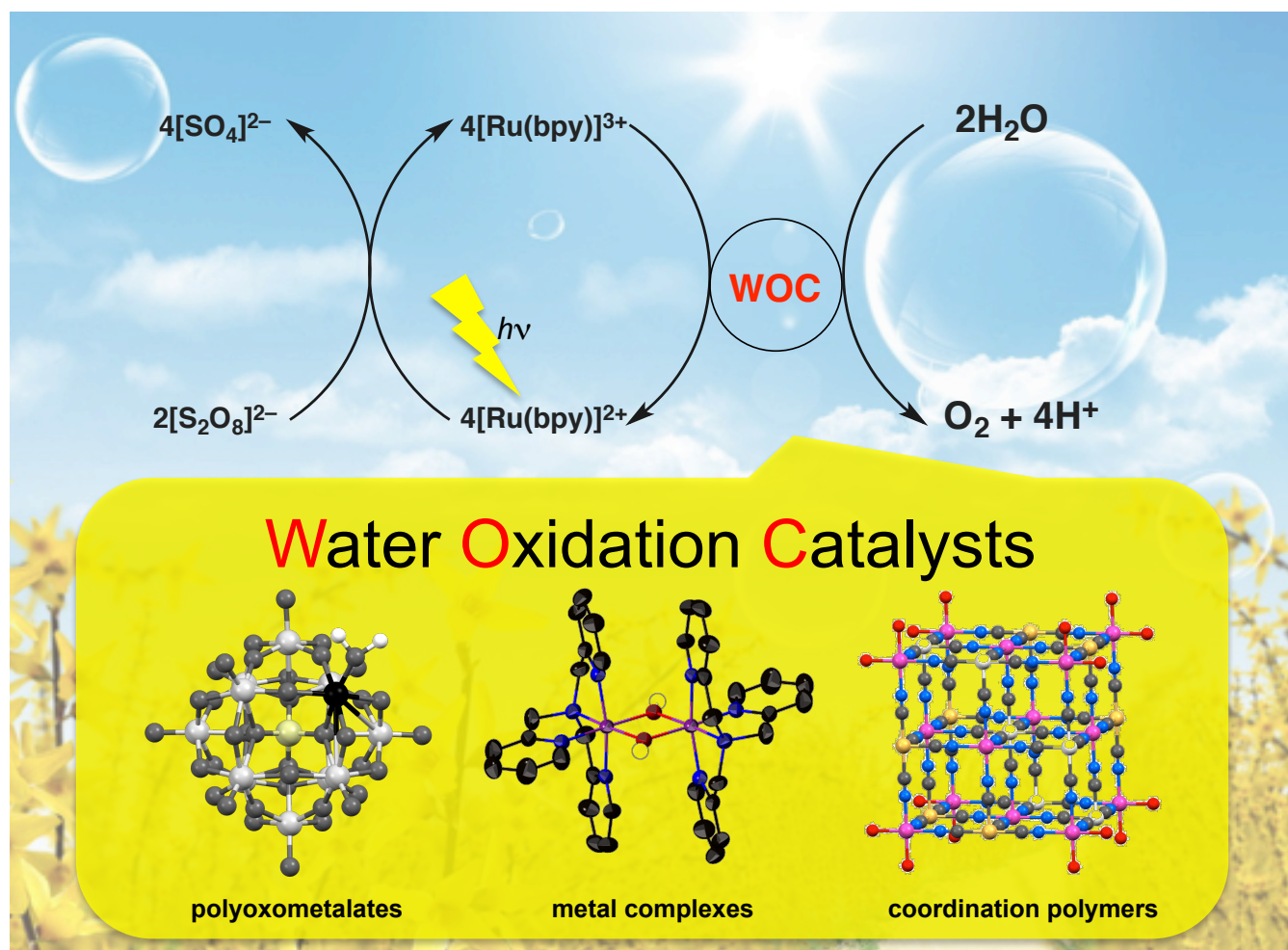
Abstract: Photocatalytic oxidation of water by persulfate ($Na_2S_2O_8$) with $[Ru(bpy)_3]^{2+}$ (bpy = 2,2'-bipyridine) as a photocatalyst provides a standard protocol to study the catalytic reactivity of water oxidation catalysts. The yield of evolved oxygen per persulfate is regarded as a good index for the catalytic reactivity because the oxidation of the ligand of $[Ru(bpy)_3]^{2+}$ competes with the catalytic water oxidation. A variety of metal complexes act as catalysts in the photocatalytic oxidation of water by persulfate with $[Ru(bpy)_3]^{2+}$ as a photocatalyst. The catalytic mechanisms are discussed in the homogeneous water oxidation catalysis. Some metal complexes are converted to metal oxide or hydroxide nanoparticles during the photocatalytic water oxidation by persulfate, acting as precursors for the actual catalysts. The catalytic reactivity of various metal oxides is compared based on the yield of evolved oxygen and turnover frequency. A heteropolynuclear cyanide complex is the best catalyst reported so far for the photocatalytic water oxidation by persulfate and $[Ru(bpy)_3]^{2+}$, affording 100% yield of O_2 per persulfate.

Introduction

The most important challenge that we are facing in the 21st century is definitely the development of artificial photosynthesis to provide sustainable energy supply using solar energy.[1-23] The photosynthesis is the process to take four electrons and four protons from water, which requires the solar energy.[24-27] The deeper understanding of the structure and function of the 'natural' photosynthetic process provides a source of insight and inspiration for discovering how solar energy can be stored in a chemical bond as a low mass, high energy carrier fuel.[4-23] The artificial photosynthesis consists of several processes composed of light-harvesting, charge-separation, and water oxidation and reduction processes, mimicking the natural photosynthesis.[4-23] The most challenging part among those processes is to develop efficient catalysts for water oxidation like the oxygen evolving complex (OEC) in photosystem II.[28-38]

$[Ru(bpy)_3]^{3+}$ (bpy = 2,2'-bipyridine) has been frequently used as an oxidant for water oxidation to study the catalytic reactivity, including photodriven catalytic water oxidation because of its ability to react as a pure one-electron oxidant, the wide range of reduction potentials accessible through ring substitution, pH independent potentials, high quantum yield of photogeneration, and characteristic absorption spectra of both $[Ru(bpy)_3]^{3+}$ and $[Ru(bpy)_3]^{2+}$, which allow the water oxidation reaction to be easily monitored using UV–vis spectrophotometer.[39,40] Production of $[Ru(bpy)_3]^{3+}$ in high quantum and chemical yields can be readily achieved through the oxidative quenching of the excited state of $[Ru(bpy)_3]^{2+}$ by persulfate ($S_2O_8^{2-}$) in an aqueous solution (Scheme 1).[40] The $SO_4^{•-}$ radical anion produced by dissociative electron transfer from $[Ru(bpy)_3]^{2+*}$ to $S_2O_8^{2-}$ can oxidize another equivalent of $[Ru(bpy)_3]^{2+}$ to $[Ru(bpy)_3]^{3+}$. Since water can be oxidized by $[Ru(bpy)_3]^{3+}$ in the presence of water oxidation catalysts, the photocatalytic water oxidation with persulfate provides a standard protocol to study the catalytic reactivity of water oxidation catalysts.

$$[Ru(bpy)_3]^{2+*} + S_2O_8^{2-} \underset{k_{-d}}{\overset{k_d}{\rightleftharpoons}} [Ru(bpy)_3]^{2+*} | S_2O_8^{2-} \overset{k_{et}}{\rightarrow}$$

$$hv \big\| 1/\tau_0 \qquad hv \big\| 1/\tau_0^{IP} \qquad [Ru(bpy)_3]^{3+} + SO_4^{2-} + SO_4^{•-}$$

$$[Ru(bpy)_3]^{2+} + S_2O_8^{2-} \overset{K_{IP}}{\rightleftharpoons} [Ru(bpy)_3]^{2+} | S_2O_8^{2-} \overset{k_{tet}}{\nearrow}$$

Scheme 1. Oxidative quenching of the excited state of $[Ru(bpy)_3]^{2+}$ by $S_2O_8^{2-}$.

The scope of the current review is to comprehensively compare the catalytic reactivity of water oxidation catalysts in the photocatalytic water oxidation by persulfate using $[Ru(bpy)_3]^{2+}$ as a photocatalyst. First, the catalytic reactivities and mechanisms of metal complexes acting as homogeneous catalysts in water oxidation reactions are compared and discussed. Then, the conversion of homogeneous catalysts to metal oxide nanoparticles during the water oxidation is discussed to clarify the actual heterogeneous catalysts produced from the precursor metal complexes in homogeneous solution. Finally the catalytic activity of various metal oxide nanoparticles is compared in the $[Ru(bpy)_3]^{2+}$-photocatalyzed water oxidation by persulfate to develop the most efficient water oxidation catalyst affording 100% yield O_2.

Homogeneous Catalysts

Extensive efforts have been devoted to develop homogeneous water oxidation catalysts (WOCs) in the photocatalytic oxidation of water by persulfate as an oxidant with $[Ru(bpy)_3]^{2+}$ as a photocatalyst.[41-66] The turnover numbers (TONs) and the yields of O_2 are summarized in Table 1. Molecular polyoxometalates (POMs) have been developed as efficient WOCs, because inorganic ligands of POMs are hardly oxidized during the water

[a] Prof. Dr. S. Fukuzumi, Dr. J. Jung, Prof. Dr. W. Nam
Department of Chemistry and Nano Science
Ewha Womans University, Seoul 120-750 (Korea)
E-mail: fukuzumi@chem.eng.osaka-u.ac.jp, wwnam@ewha.ac.kr

[b] Prof. Dr. S. Fukuzumi
Faculty of Science and Engineering, Meijo University, ALCA and
SENTAN, Japan Science and Technology Agency (JST), Nagoya, Aichi
468-0073 (Japan)

[c] Prof. Dr. S. Fukuzumi
Graduate School of Engineering, Osaka University, ALCA and
SENTAN, Japan Science and Technology Agency (JST), Suita, Osaka
565-0871 (Japan)

[d] Prof. Dr. Y. Yamada
Department of Applied Chemistry and Bioengineering, Graduate
School of Engineering, Osaka City University, 3-3-138 Sugimoto,
Sumiyoshi, Osaka 558-8585 (Japan)
E-mail: ymd@a-chem.eng.osaka-cu.ac.jp

[e] Prof. Dr. T. Kojima
Department of Chemistry, Faculty of Pure and Applied Science
University of Tsukuba, 1-1-1 Tennodai,
Tsukuba 305-8571 (Japan)
E-mail: kojima@chem.tsukuba.ac.jp

Table 1. TON and yield in photocatalytic oxidation of water by persulfate using homogeneous catalysts.

Catalyst	pH	TON[a]	Yield (%)[b]	Ref
$[Fe_{11}(H_2O)_{14}(OH)_2(W_3O_{10})_2(\alpha\text{-}SbW_9O_{33})_6]^{27-}$[c]	10.0	1815	94	41
$[Co^{II}_3Ho(hmp)_4(OAc)_5H_2O]$[d,e]	8.0	99	97	42
$[Co^{II}_3Er(hmp)_4(OAc)_5H_2O]$[d,e]	8.0	93	91	42
$[Co^{II}_3Tm(hmp)_4(OAc)_5H_2O]$[d,e]	8.0	40-72	>90	42
$[Co^{II}_3Yb(hmp)_4(OAc)_5H_2O]$[d,e]	8.0	76	97	42
$[Co^{II}_4(hmp)_4(\mu\text{-}OAc)_2(\mu_2\text{-}OAc)_2(H_2O)_2]$[d,e]	8.0	29	96	43
$[(A\text{-}\alpha\text{-}SiW_9O_{34})_2Co_8(OH)_6(H_2O)_2(CO_3)_3]^{16-}$ (Co₈POM)	9.0	1436	44	44
$[\{Ru_4O_4(OH)_2(H_2O)_4\}(\gamma\text{-}SiW_{10}O_{36})_2]^{10-}$	7.2	350	38	45
$Na_{50}[Ni_{25}(H_2O)_2(OH)_{18}(CO_3)_2(PO_4)_6(SiW_9O_{34})_6]\cdot 85H_2O$	9.0	125	18	46
$[\{Co_4(OH)_3(PO_4)\}_4(GeW_9O_{34})_4]^{32-}$	9.0	39	31	47
$[\{Co_4(OH)_3(PO_4)\}_4(AsW_9O_{34})_4]^{28-}$	9.0	33	26	47
$Na_{10}[Co_4(H_2O)_2(VW_9O_{34})_2]\cdot 35H_2O$	9.0	750	60	48
$Co_3(O_3PCH_2\text{-}NC_4H_7\text{-}CO_2)_2\cdot 4H_2O$	9.0	10	78	49
$[Mn^{III}_3Mn^{IV}O_3(CH_3COO)_3(A\text{-}\alpha\text{-}SiW_9O_{34})]^{6-}$	5.2	5.2	3.7	50
$K_{10}[Co(H_2O)_2(\gamma\text{-}SiW_{10}O_{35})_2]\cdot 23H_2O$	9.0	187	58	51
$Cs_9[(\gamma\text{-}PW_{10}O_{36})_2Ru^{IV}_4O_5(OH)(OH_2)_4]$	5.8	120	25	52
$(NH_4)_3[CoMo_6O_{24}H_6]\cdot 7H_2O$	8.0	107	26	53
$(NH_4)_6[Co_2Mo_{10}O_{38}H_4]\cdot 7H_2O$	8.0	154	20	53
$[Co^{II}(Py5OH)(Cl)](BF_4)$[f]	8.0	51	34	54
$[Co_2(spy)_2](ClO_4)_4$[g]	8.5	442	5.6	55
CoTPPS[h]	11	122	49	56
CoFPS[i]	9.0	570	60	57
$[Co(qpy)(OH_2)_2]^{2+}$[j]	8.0	160	67	58
$[Ru(bda)(ppy)_2]$[k]	7.1	267	80	59
$[Ru(bda)L_2]$[l]	7.0	518	50	60
$[Ru(bda)L_2]\text{-}[(Ru(bpy)_3)^{2+}]_2$[m]	7.0	210	41	61
$[Ru(NPM)(H_2O)(pic)_2]^{2+}$[n]	7.0	103	18	62
$[Fe(TAML)]^-$[o]	8.7	220	44	63
$[(V^{IV}_5V^V_1)O_7(OCH_3)_{12}]^-$	7.0	67	20	64
$Na[\{Ru^{II}(py\text{-}SO_3)_2(H_2O)\}_2(\mu\text{-}Mebbp)]$	7.0	5300	22	65
$[Co_2(\mu\text{-}OH)_2(TPA)_2](ClO_4)_4$[p]	9.3	742	72	66

[a] TON is defined as the total number of moles of O_2 per mole of the catalyst. [b] Yield is defined as twice the number of moles of O_2 per mole of $Na_2S_2O_8$. [c] LED lamp ($\lambda \geq 420$ nm), 1.0 mM $[Ru(bpy)_3](ClO_4)_2$ (1.0 mM), $Na_2S_2O_8$ (5.0 mM), total reaction volume is 16 mL and overall volume is ca. 21 mL, sodium borate buffer (80 mM, initial pH 10.0), and vigorous agitation using a magnetic stirrer. Room temperature: 25 °C. [d] hmp = 2-(hydroxymethyl)pyridine. [e] Typical conditions: a 470 nm high flux LED (26.1 mW/cm²), $[Ru(bpy)_3]^{2+}$ (1.0 mM), $Na_2S_2O_8$ (5.0 mM), 8 mL of a borate buffered solution (pH = 8.0). [f] Py5 = 2,6-bis(methoxydi(pyridin-2-yl)methyl)pyridine. [g] spy = 2,2':6',2'':6'',2''':6''',2''''-sexipyridine. [h] CoTPPS = (5,10,15,20-tetrakis(4'-sulfonatophenyl)porphinato) cobalt(II) tetra sodium salt. [i] CoFTS = a fluorinated cobalt porphyrin. [j] qpy = 2,2':6',2'':6'',2'''-quaterpyridine. [k] H₂bda = 2,2'-bipyridine-6,6'-dicarboxylic acid; ppy = 4-phenylpyridine. [l] L = N-cyclic aromatic ligands. [m] Two Ru(II)-polypyridine photosensitizers are covalently linked to one $[Ru(bda)L_2]$

catalyst. [n] NPM = 4-tert-butyl-2,6-di-(1',8'-naphthyrid-2'-yl)pyridine, pic = 4-picoline. [o] TAML = tetraamido macrocyclic ligand. [p] TPA = tris(2-pyridylmethyl)amine.

Shunichi Fukuzumi earned a bachelor's degree and PhD degree in applied chemistry at Tokyo Institute of Technology in 1973 and 1978, respectively. After working as a postdoctoral fellow (1978-1981) at Indiana University in USA, he joined the Department of Applied Chemistry, Osaka University, as an Assistant Professor in 1981 and was promoted to a Full Professor in 1994. His research interests are artificial photosynthesis and electron transfer chemistry. He is now a Distinguished Professor of Ewha Womans University, a Designated Professor of Meijo University, a Professor Emeritus of Osaka University, and the leader of an ALCA (Advanced Low Carbon Technology Research and Development) project that started in 2011.

Jieun Jung earned a bachelor's degree from Chungnam National University, Korea in 2010, and PhD degree from Osaka University, Japan in 2015. She is now working as a postdoctoral fellow at Ewha Womans University.

Yusuke Yamada earned his PhD degree in macromolecular science from Osaka University in 1998. He was working as a researcher and senior researcher at Osaka National Research Institute (currently AIST) from 1998 to 2009. From 2007 to 2008, he was a visiting scholar at UC Berkeley. He was an associate professor of Osaka University from 2009. In 2015, he moved to Osaka City University as a Professor.

Takahiko Kojima is a Professor of the Department of Chemistry at University of Tsukuba. He received his BE (1986) and PhD (1991) from the University of Tokyo. After post-doctoral work at University of Minnesota, USA, he became a Research Associate at the Department of Chemistry at Kyushu University in Japan in 1994, and then moved to Osaka University as an Associate Professor in 2005. In 2008, he moved to Tsukuba. His research interest involves bioinspired redox chemistry of ruthenium complexes and development of functional π-space based on non-planar π-systems.

Wonwoo Nam received his BS (Honors) degree in Chemistry at California State University, Los Angeles (1985), and his PhD degree in Inorganic Chemistry at UCLA (1990). After one year postdoctoral experience at UCLA, he became an Assistant Professor at Hong Ik University in 1991. He moved to Ewha Womans University in 1994, where he is presently a Distinguished Professor of Ewha Womans University. His current research focuses on the dioxygen activation, water oxidation, and sensors for metal ions in bioinorganic chemistry.

oxidation.[67-69] An iron-based POM, $[Fe_{11}(H_2O)_{14}(OH)_2(W_3O_{10})_2$-$(\alpha\text{-}SbW_9O_{33})_6]^{27-}$ (Figure 1), acts as the most efficient catalyst in the $[Ru(bpy)_3]^{2+}$-photocatalyzed water oxidation by persulfate, affording a high TON (1815) and a high O_2 yield per persulfate (94%) at pH 10 in a sodium borate buffer aqueous solution.[41] The O_2 yield is defined as twice the number of moles of O_2 per mole of $Na_2S_2O_8$, because two moles of $Na_2S_2O_8$ are required for the four-electron oxidation of H_2O to evolve O_2. The catalytic cycle of visible light-driven water oxidation by persulfate and $[Ru(bpy)_3]^{2+}$ is shown in Scheme 2. $[Ru(bpy)_3]^{3+}$ produced by oxidative electron-transfer quenching of $[Ru(bpy)]^{2+*}$ by persulfate (Scheme 1) can oxidize water by the catalysis of a WOC (Scheme 2).
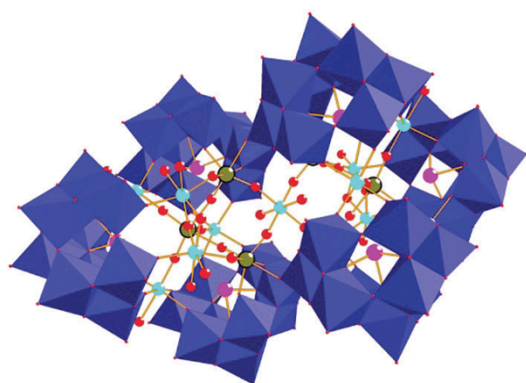
Figure 1. Structure of $[Fe_{11}(H_2O)_{14}(OH)_2(W_3O_{10})_2(\alpha\text{-}SbW_9O_{33})_6]^{27-}$: $[\alpha\text{-}SbW_9O_{33}]^{9-}$ polyhedra (blue), Fe (cyan), O/H$_2$O/OH (red), Sb (pink), W (dark yellow).
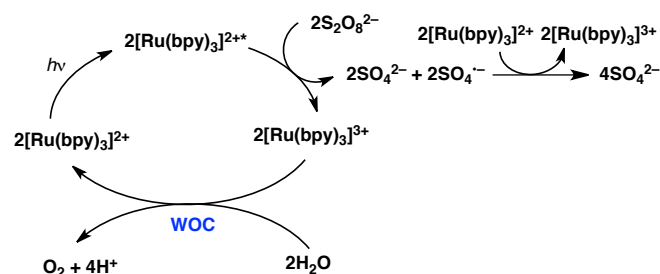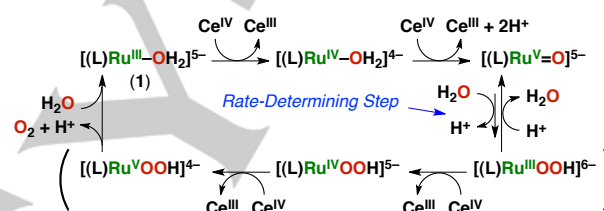

Scheme 2. Photocatalytic cycle for water oxidation by persulfate with $[Ru(bpy)_3]^{2+}$ and WOC.

The initial reaction rate of 7.9 mmol min^{-1} (the oxygen evolution rate in the first 60 s of light illumination) and TOF$_{initial}$ (TON 1 min/60 s) of 6.3 s^{-1} in the photocatalytic oxidation with the Fe-POM are the largest among the data in Table 1.[41] The quantum yield [(initial O_2 formation rate)/(photon flux)] of 47% is also the highest value ever reported for the homogeneous photocatalytic water oxidation, because the quantum yield 50% corresponds to 100% quantum efficiency (two photons are required to produce four equivalents of $[Ru(bpy)_3]^{3+}$, which oxidize water to O_2 with WOC).[41] Isotope-labeling water oxidation experiments using ^{18}O-enriched water instead of $H_2{}^{16}O$ demonstrated that the evolved oxygen comes from water oxidation.[41] In catalytic water oxidation, homogeneous metal complexes are often claimed as precatalysts, which decompose

under oxidizing conditions to insoluble metal oxides that are the real catalysts as discussed in the next section. Dynamic light scattering (DLS) measurements indicate that no nanoparticles were produced during the photocatalytic water oxidation with the POM, which remains as a soluble homogeneous catalyst.[41]

Inspired by the {CaMn$_4$O$_5$} oxygen evolving complex of photosystem II where Ca^{2+} plays the essential role,[70,71] the $[Co^{II}{}_3Ln(hmp)_4(OAc)_5H_2O]$ (Ln = Ho $-$ Yb, hmp = 2-(hydroxymethyl)pyridine) cubane complexes were designed to address crucial design parameters, ranging from nuclearity and redox-inactive promoters by newly combining Ln^{3+} centers as redox-inactive Ca^{2+} analogues with flexible aqua-/acetate ligands into active and stable WOCs, which afforded high O_2 yields in the photocatalytic water oxidation by persulfate (Table 1).[42,43]

The catalytic mechanism was reported for the water oxidation by ceric ammonium nitrate (CAN), $(NH_4)_2[Ce^{IV}(NO_3)_6]$, using all-inorganic mononuclear ruthenium complexes bearing a Keggin-type lacunary heteropolytungstate, $[Ru^{III}(H_2O)SiW_{11}O_{39}]^{5-}$ and $[Ru^{III}(H_2O)GeW_{11}O_{39}]^{5-}$, as WOCs.[72] It has been proposed that Ru^V=O species was produced by the two-electron oxidation of the Ru^{III} complex with two equivalents of CAN (Scheme 3).[72] The formation of the Ru^V=O complex was indeed detected by EPR and resonance Raman spectroscopy.[72] A kinetic study suggested that the rate-determining step (r.d.s.) is the nucleophlic attack of H_2O to the Ru^V=O complex to produce the Ru^{III}OOH complex, which is the O–O bond formation step, where the reverse O–O bond cleavage process is in competition with the follow-up two- electron oxidation processes to generate O_2 (Scheme 3).[72]

Scheme 3. Catalytic cycle for thermal water oxidation with CAN using $[(L)Ru^{III}\text{-}OH_2]$, ($[Ru^{III}(H_2O)SiW_{11}O_{39}]^{5-}$ and $[Ru^{III}(H_2O)GeW_{11}O_{39}]^{5-}$), as WOCs.

Virtually, the same mechanism, as shown in Scheme 4, was proposed for the photocatalytic water oxidation by persulfate using a water-soluble cobalt porphyrin (CoFPS), which possesses fluorine groups at the 2- and 6-positions of the *meso*-aryl rings of the porphyrin (Scheme 4).[57] CoFPS exhibited significantly improved stability with a high TON (570), as compared with non-fluorinated Co porphyrin (CoTPPS: TON = 122).[56] The increased stability results from resistance of CoFPS against singlet oxygen, the formation of which was monitored in situ by using 9,10-diphenylanthracene as a chemical probe.[57] DLS indicated that CoFPS remained homogeneous during the water oxidation catalysis.[57] In the case of the photocatalytic oxidation, two equivalents of $[Ru(bpy)_3]^{3+}$ produced by the oxidative quenching of $[Ru(bpy)_3]^{2+*}$ by persulfate (Scheme 1) can oxidize Co^{III}FPS to produce Co^{IV}(O)FPS$^{\bullet+}$, which is
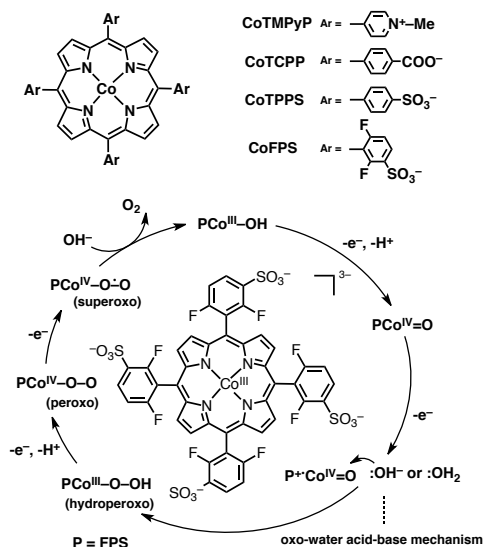
Scheme 4. Catalytic cycle for photodriven water oxidation by persulfate using CoFPS as a WOC.

equivalent to $Co^V(O)FPS$ (Scheme 4). The nucleophilic attack of water to $Co^V(O)FPS$ affords the hydroperoxo complex ($[Co^{III}(OOH)FPS]^-$), which is further oxidized by two equivalents of $[Ru(bpy)_3]^{3+}$ to produce O_2 and regenerate $Co^{III}FPS$ (Scheme 4).[57] The nucleophilic attack of water to high-valent cobalt-oxo species have also been proposed for electrocatalytic oxidation of water with Co hangman corroles,[73] non-heme Co complexes,[74] and cationic Co porphyrins.[75]

When a Ru^{III}-aqua complex, $Ru(\kappa_3^{O,N,N}bda)(L)_2(OH_2)$ (L = 6-F-isoquinoline), was employed as a WOC for the water oxidation by CAN, a $Ru^V=O$ species produced by the oxidation of Ru^{III}-OH_2 by two equivalents of CAN was proposed to undergo radical coupling to produce the dinuclear peroxo complex (Ru^{IV}-O-O-Ru^{IV}), as shown in Scheme 5.[76] O_2 may be evolved directly by the reaction of Ru^{IV}-O-O-Ru^{IV} with water or Ru^{IV}-O-O-Ru^{IV} is further oxidized to a superoxo complex which reacts with H_2O to evolve O_2, accompanied by regeneration of Ru^{III}-OH_2 and Ru^{IV}-OH (Scheme 5). The radical coupling process may be the rate-determining step in the catalytic water oxidation with CAN, because the rate of water
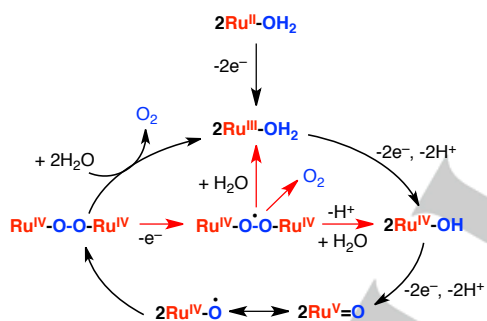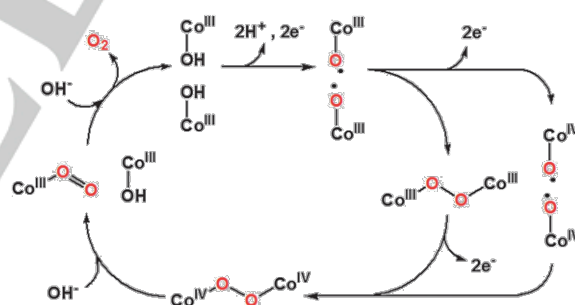
oxidation was proportional to square of concentration of Ru^{III}-OH_2.[76] The formation of the radical superoxo intermediate $[Ru^{IV}-O-O-Ru^{IV}]^{\cdot 3+}$ was indicated in the electrochemical experiments and supported by DFT calculations.[76] However, the direct detection of the intermediates has yet to be made. $[Ru(bda)(6-fluoroisoquinoline)_2]$ showed an extremely high catalytic activity with a TOF of 1000 s^{-1}, whereas $[Ru(bda)(6-bromophthalazine)_2]$ exhibited a high TON (~100,000).[76]

A large TON (5300) was obtained in the photocatalytic oxidation of water by persulfate with a ruthenium tris(bipyridyl)-type dye (RuPS) and a pyrazolate-based dinuclear ruthenium water oxidation catalyst, $\{[Ru^{II}(py-SO_3)_2(H_2O)]_2(\mu-Mebbp)\}^-$, at pH 7.0 (Table 1).[65,77] The mechanism of O-O bond formation (nucleophilic attack of water in Schemes 3 and 4 vs. radical coupling in Scheme 5) in the catalytic water oxidation can be controlled by the relative position of the Ru-O units, in addition to the electronic effects exerted by the auxiliary ligands.[13,78-80]

A radical coupling mechanism was also proposed for the O-O bond formation in the photocatalytic oxidation of water by persulfate with $[Ru(bpy)_3]^{2+}$ and CoTPPS, as shown in Scheme 6.[56] The observation of a second-order dependence of the rate on concentration of CoTPPS in the photocatalytic water oxidation by persulfate indicates that the radical coupling of two Co-oxyl radicals is the rate-determining step in Scheme 6.[56] The change in the O-O bond formation mechanism from the nucleophilic attack of water to the $Co^V(O)$ species (or $Co^{IV}(O)$ porphyrin radical cation) of CoFPS in Scheme 4 to the radical coupling of the $Co^{IV}(O)$ species of CoTPPS in Scheme 6 was suggested on the basis of the observation of less steric effect in CoTPPS relative to CoFPS owing to the shift of the sulfate groups from the 3- to 4-positions on the aryl rings for the bimolecular radical coupling reaction.[57] The calculated Mulliken spin densities at the oxo ligand for the formally Co^V complexes show that CoFPS has more radical character on the oxyl oxygen (spin = 1.42) than CoTPPS does (spin = 1.09), thus suggesting that CoFPS may be more efficient at bimolecular radical coupling.[57] However, the electronic effect seems to be less important in the catalytic water oxidation with cobalt porphyrins. Any intermediates in Scheme 6 have yet to be detected or identified.

A bis-hydroxo-bridged dinuclear Co^{III}-pyridylmethylamine complex, $[\{Co(TPA)\}_2(\mu-OH)_2]^{4+}$ (**1**), acts as a homogeneous

Scheme 5. Catalytic cycle for water oxidation by CAN with a Ru^{III}-aqua complex ($Ru-OH_2$: $[Ru(\kappa_3^{O,N,N}bda)(L)_2(OH_2)]$ (L = 6-F isoquinoline)).

Scheme 6. Catalytic cycle for photodriven water oxidation by persulfate with $[Ru(bpy)_3]^{2+}$ as a photocatalyst and CoFPS as a WOC.
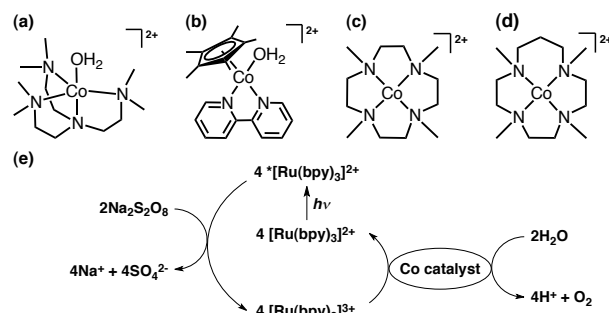
catalyst for photocatalytic water oxidation by persulfate with [Ru(bpy)$_3$]$^{2+}$, affording a high quantum yield (88%) and chemical yield (72%) with a high turnover number (TON = 742) for O$_2$ formation (Table 1) without forming catalytically active Co-oxide (CoO$_x$) nanoparticles.[66] The pH dependence of the catalytic activity indicates that the active species of water oxidation is a species (**2**) derived from the two-electron PCET oxidation of **1** and the PCET formation of **2** is the rate-determining step of the water oxidation, as shown in Scheme 7.[66] The DFT calculations suggest that the most stable state of **2** is the triplet state of the bis-μ-oxyl Co^{III}-dinuclear complex, [Co$^{III}_2$(μ-O$^{\bullet-}$)$_2$(TPA)$_2$]$^{4+}$, rather than a bis-μ-oxo-Co^{IV} dinuclear complex.[66] The bis-μ-oxyl-Co$^{III}_2$ complex in the singlet state is thermally accessible on the basis of the result suggesting that the singlet species is only 0.5 kcal mol^{-1} higher than the triplet state, being converted thermally to a putative μ:η^2,η^2-peroxo-Co^{III} dinuclear complex, the energy of which is only by 0.7 kcal mol^{-1} higher than that of the singlet bis-μ-oxyl-Co$^{III}_2$ complex.[66] Based on isotope-labeling experiments, the O-O bond formation has been proposed to occur via intramolecular radical coupling between the two oxyl ligands locating diagonally in the singlet Co$^{III}_2$(μ-O$^{\bullet-}$)$_2$ rectangular core to afford the putative μ:η^2,η^2-peroxo-Co^{III} intermediate, which reacts with water to produce a proposed μ-peroxo-μ-hydroxo dinuclear Co^{III} complex (**3**).[66] The complex **3** is further oxidized to evolve O$_2$, accompanied by regeneration of **1** (Scheme 7).[66]
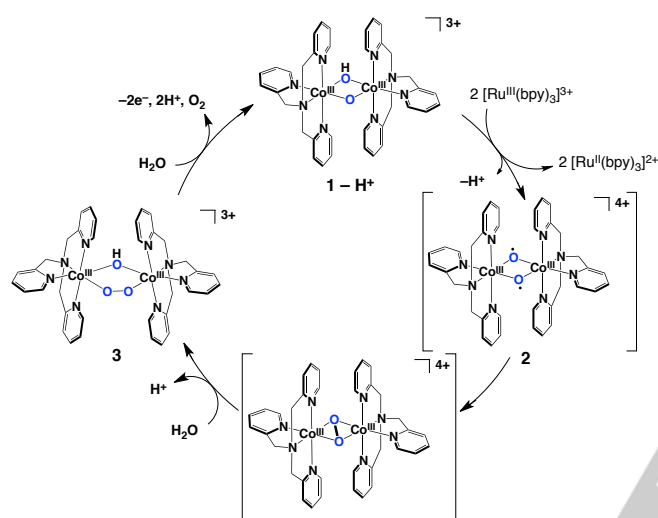
Scheme 7. Catalytic cycle for photodriven water oxidation at pH 9.3 by persulfate with [Ru(bpy)$_3$]$^{2+}$ as a photocatalyst and a bis-μ-hydroxo-Co^{III}-TPA dinuclear complex, [{Co(TPA)}$_2$(μ-OH)$_2$]$^{4+}$ (**1**), as a WOC. At pH 9.3, the complex **1** is deprotonated to be the corresponding μ-oxo-μ-hydroxo form (**1 – H$^+$**).

Homogeneous *vs.* Heterogeneous Catalysts

As mentioned above, determination of the true catalyst for the oxidation of water to dioxygen has become an important issue because extra caution needs to be taken to clarify whether

Figure 2. Chemical structures of mononuclear water-soluble cobalt complexes uses as precatalysts (a) [Co^{II}(Me$_6$tren)(OH$_2$)]$^{2+}$, (b) [Co^{III}(Cp*)(bpy)(OH$_2$)]$^{2+}$, (c) [Co^{II}(12-TMC)]$^{2+}$, and (d) [Co^{II}(13-TMC)]$^{2+}$. (e) A scheme showing the overall catalytic cycle for photocatalytic water oxidation by Na$_2$S$_2$O$_8$ with [Ru(bpy)$_3$]$^{2+}$ and a cobalt complex precatalyst.

nanoparticles are produced from the homogeneous metal complexes throughout the oxidation reactions, acting as the actual catalysts or not.[81-93] Water soluble cobalt complexes (Figures 2a-d) have been reported to act as precatalysts rather than actual catalysts in the photocatalytic oxidation of water by persulfate with [Ru(bpy)$_3$]$^{2+}$.[94] The TON and yield of O$_2$ are listed in Table 2. The yield of O$_2$ per persulfate with [Co^{II}(Me$_6$tren)(OH$_2$)]$^{2+}$ (50 μM) was 54%.[94] When the concentration of [Co^{II}(Me$_6$tren)(OH$_2$)]$^{2+}$ was increased to 2.5 mM, however, no O$_2$ was evolved after photoirradiation of the buffer solution containing Na$_2$S$_2$O$_8$ and [Ru(bpy)$_3$]$^{2+}$ (1st run), because the oxidation of the organic ligands proceeded prior to water oxidation to produce CO$_2$ rather than O$_2$.[94] Particles formed at the 1st run were separated from the reaction solution by centrifugation, washed with water and ethanol successively and dried in vacuo at room temperature.[94] When the particles (~0.12 mg) were employed as a catalyst at the 2nd run, efficient O$_2$ evolution (~60% yield) was observed.[94] The robustness of the collected nanoparticles was confirmed by using them for further reaction cycle when a significant amount of O$_2$ evolution (yield: 47%) was observed in the 3rd run.[94] Thus, the actual catalyst for the photocatalytic water oxidation was the particles derived from [Co^{II}(Me$_6$tren)(OH$_2$)]$^{2+}$.[94] The nanoparticle formation was confirmed by DLS measurements, which indicate that the average size of nanoparticles is 15 – 60 nm.[94] Transmission electron microscopy (TEM) images of the particles derived from [Co^{II}(Me$_6$tren)(OH$_2$)]$^{2+}$ are displayed in Figures 3a and 3b.[94] The size of particles ranged from 10 to 50 nm, which agree with the particles sizes determined by DLS (15 – 60 nm).[94] Similar nanoparticles were formed from [Co^{III}(Cp*)(bpy)(OH$_2$)]$^{2+}$ (Figures 3c and 3d) and Co(NO$_3$)$_2$ (Figures 3e and 3f).[94] The high magnification image in Figure 3b indicates that smaller particles in the size of few nanometers were also formed, indicating that the particles observed in Figure 3a are secondary particles.[94]

X-ray photoelectron spectroscopy (XPS) spectra of the nanoparticles derived from [Co^{II}(Me$_6$tren)(OH$_2$)]$^{2+}$ exhibited Co 2p$_{1/2}$ and Co 2p$_{3/2}$ peaks at 780.0 eV and 795.3 eV, respectively, with weak satellite peaks.[94] Co$_3$O$_4$ also showed two intense peaks at 779.8 eV for Co 2p$_{1/2}$ and at 795.1 eV for Co 2p$_{3/2}$ with weak satellite peaks.[94] Slightly intense satellite peaks observed with the nanoparticles were ascribed to the higher ratio of Co(II)

Table 2. TON and yield in photocatalytic oxidation of water by persulfate using homogeneous catalyst precursors.

Catalyst	pH	TON[a]	Yield (%)[b]	Ref
$[Co^{II}(Me_6tren)(OH_2)]^{2+[c,d]}$	8.0	54	54	94
$[Co^{III}(Cp^*)(bpy)(OH_2)]^{2+[c,e]}$	8.0	29	29	94
$[Co^{II}(12\text{-}TMC)]^{2+[c,f]}$	8.0	16	16	94
$[Co^{II}(13\text{-}TMC)]^{2+[c,g]}$	8.0	41	41	94
$Co^{II}(NO_3)_2^{[c]}$	8.0	52	52	94
$Co^{II}(Salen)^{[h]}$	9.0	854	55	95
$Fe(mcp)Cl_2^{[i]}$	8.5	194	24	97
$[Fe(bpy)_2Cl_2]Cl$	8.5	157	21	97
$[Fe(tpy)_2]Cl_2^{[j]}$	8.5	376	42	97
$[Fe(cyclen)Cl_2]Cl^{[k]}$	8.5	412	46	97
$Fe(tmc)Br_2^{[l]}$	8.5	364	41	97
$Fe(ClO_4)_3$	8.5	436	48	97
$Fe(BQEN)(OTf)_2^{[m]}$	9.0	259	52	98
$[NiL_1](ClO_4)_2^{[n]}$	8.0	2	3	100
$[NiL_2](ClO_4)_2^{[o]}$	8.0	53	30	100
$[NiL_3](ClO_4)_2^{[p]}$	8.0	54	31	100
$[NiL_4](ClO_4)_2^{[q]}$	8.0	31	19	100
$[NiL_5](ClO_4)_2^{[r]}$	8.0	41	25	100
$[NiL_6](ClO_4)_2^{[s]}$	8.0	50	29	100
$Ni(NO_3)_2$	8.0	65	37	100

[a] TON is defined as the total number of moles of O_2 per mole of the catalyst. [b] Yield is defined as twice the number of moles of O_2 per mole of $Na_2S_2O_8$. [c] Typical conditions: Photoirradiation (Xe lamp, $\lambda > 420$ nm) of a buffer solution (2.0 mL, 50 mM phosphate, pH 8.0) containing $[Ru(bpy)_3]^{2+}$ (0.50 mM), $Na_2S_2O_8$ (10 mM) and a mononuclear cobalt complex (50 μM). [d] Me_6tren = tris[2-(dimethylamino)ethyl]amine. [e] Cp^* = pentamethylcyclopntadienyl. [f] 12-TMC = 1,4,7,10-tetramethyl-1,4,7,10-tetraazacyclododecane. [g] 13-TMC = 1,4,7,10-tetramethyl-1,4,7,10-tetraazacyclotridecane. [h] Salen = N,N'-bis(salicylidene)ethylenediamine. [i] mcp = N,N'-dimethyl-N,N'-bis(2-pyridylmethyl)cyclohexane-1,2-diamine. [j] tpy=2,2':6',2''-terpyridine. [k] cyclen=1,4,7,10-tetraazacyclododecane. [l] tmc = 1,4,8,11-tetramethyl-1,4,8,11-tetraazacyclotetradecane. [m] BQEN = N,N'-dimethyl-N,N'-bis(8-quinolyl)ethane-1,2-diamine. [n] L_1 = $N,N,N'N'$-tetrakis(2-pyridylmethyl)ethylenediamine. [o] L_2 = N,N,N'-tris-[2-(2'-pyridyl)ethyl]-N'-methylethane-1,2-diamine. [p] L_3 = N,N'-bis-[2-(2'-pyridyl)ethyl]-N,N'-dimethylethane-1,2-diamine. [q] L_4 = N,N'-dimethyl-N,N'-bis(pyridyl-2yl-methyl)ethylene-diamine. [r] L_5 = meso-2,3,7,11,12-pentamethyl-3,7,11,17-tetra-azabicyclo[11.3.1]heptadeca-1(17),13,15-triene. [s] L_6 = 1,4,8,11-tetramethyl-1,4,8,11-tetraazacyclotetradecane.

species before the photocatalytic water oxidation.[94] The O 1s peak of the nanoparticles appeared at 531.5 eV, which is in higher binding energy region compared with the O 1s peak of Co_3O_4 (530.3 eV) by 1.2 eV.[94] An increase in the binding energy of the O 1s peak of the nanoparticles suggests the existence of metal hydroxide species.[94] Thus, the surface of the nanoparticles derived from $[Co^{II}(Me_6tren)(OH_2)]^{2+}$ under the photocatalytic water oxidation is mainly composed of $Co(OH)_x$, which acts as the actual reactive catalyst for the photocatalytic water oxidation.[94] The organic ligands were oxidized to CO_2 during the photocatalytic water oxidation, but the carbonaceous residues may act as a modifier or capping agent of the
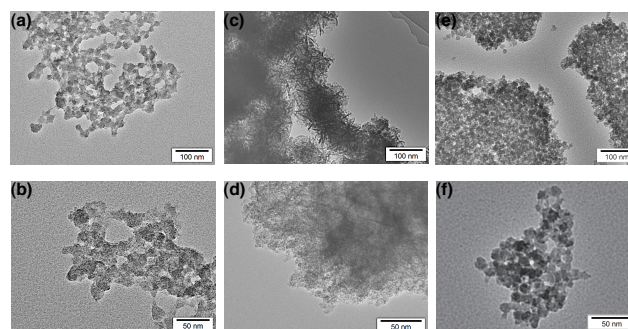
Figure 3. TEM images of nanoparticles formed during the photocatalytic water oxidation with (a and b) $[Co^{II}(Me_6tren)(OH_2)]_{2+}$, (c and d) $[Co^{III}(Cp^*)(bpy)(OH_2)]^{2+}$, and (e and f) $Co(NO_3)_2$ in a buffer solution (pH 9) containing $[Ru(bpy)_3]^{2+}$ (0.50 mM) and $Na_2S_2O_8$ (10 mM).

species compared with the authentic Co_3O_4 sample, because $[Co^{II}(Me_6tren)(OH_2)]^{2+}$ exclusively contained Co(II) nanoparticles to avoid the further aggregation to maintain the catalytic reactivity.[94]

A Co^{II}(salen) complex (salen = N,N'-bis(salicylidene)-ethylenediamine) also acts as a highly efficient water oxidation precatalyst in the photocatalytic oxidation of water by persulfate with $[Ru(bpy)_3]^{2+}$ as a photocatalyst, affording a TON of 854 at pH = 9.0 (Table 2).[95] Based on the electrospray ionization mass spectrum (ESI-MS), ^{1}H NMR and XPS analyses, the precipitates derived from Co^{II}(salen) during the photocatalytic water oxidation are composed of a mixture of Co(III) containing oxide and/or Co(III) hydroxide.[95] Cobalt-salen complexes were also reported to serve as precursors to deposit nanostructured amorphous catalyst films for catalytic water oxidation with high activity.[96]

Various iron complexes and $Fe(ClO_4)_3$ also act as precatalysts for the photocatalytic water oxidation by persulfate with $[Ru(bpy)_3]^{2+}$ at pH 8.5 to produce nanoparticles (Table 2), which were isolated and found to be Fe_2O_3 using various techniques, including energy-dispersive X-ray spectroscopy and XPS.[97] α-Fe_2O_3 nanoparticles were prepared with the diameter of 15 – 70 nm exhibited a similar catalytic reactivity with a TON of 58 to $Fe(ClO_4)_3$ used as a precatalyst which gave a TON of 57.[97]

In the case of $Fe(BQEN)(OTf)_2$ used as a precatalyst, nanoparticles isolated after the light-driven water oxidation by persulfate at the initial pH 9.0 were found to be iron hydroxides by XPS measurements.[98] Under acidic conditions, $Fe^{II}(BQEN)^{2+}$ is oxidized by two equivalents of CAN to produce an iron(IV)-oxo species, $[Fe^{IV}(O)(BQEN)]^{2+}$, which is further oxidized to produce O_2.[98] Thus, $Fe^{II}(BQEN)^{2+}$ acts as a homogeneous catalyst for water oxidation by CAN without formation of nanoparticles, although the dissociation of the BQEN ligand competes with the formation of $[Fe^{IV}(O)(BQEN)]^{2+}$ under acidic conditions.[98] Simple cobalt salts are reported to act as homogeneous catalysts for the photocatalytic water oxidation by persulfate under acidic conditions (pH 3.0), although the catalytic reactivity is much reduced as compared with that under basic conditions, where the catalytically more active nanoparticles are produced.[99]

A number of Ni complexes and salts in Table 2 were also converted to nanoparticles during the photocatalytic oxidation of water by persulfate pH 7 – 9 in borate buffer, which were found to be partially reduced β-NiOOH by scanning electron microscope (SEM), energy-dispersive X-ray spectroscopy, XPS, X-ray diffraction (XRD), and IR spectroscopies.[100] [Ni(en)$_3$]Cl$_2$ (en = 1,2-diaminoethane) was also reported to serve as a precursor to deposit nanostructured amorphous nickel oxide (NiO$_x$), which acts as water oxidation catalysts with high catalytic activity in a 0.10 M borate buffer solution (pH = 9.2).[101]

In contrast to iron complexes which act as homogeneous catalysts for water oxidation by CAN under acidic conditions (vide supra), iridium complexes [Ir^{III}(Cp*)(4,4'-R$_2$-2,2'-bipyridine)(H$_2$O)]$^{2+}$ (R = OH, OMe, Me or COOH) are converted to nanoparticles during the water oxidation by CAN.[80] The nanoparticles were composed of iridium hydroxide with a small amount of carbonaceous residue based on TG/DTA and XPS measurements of nanoparticles produced after the water oxidation.[80] The iridium hydroxide nanoparticles act as an excellent catalyst for the water oxidation by CAN with a high TOF (0.75 s^{-1}) and a high TON (>1500).[80]

A water-soluble Ir complex [Ir(Cp*)(H$_2$O)$_3$]$^{2+}$ was used as a precatalyst for iridium hydroxide nanoparticles, which acts as an efficient water oxidation catalyst in the photocatalytic oxidation of water by O$_2$ to produce hydrogen peroxide with [Ru^{II}(Me$_2$phen)$_3$]$^{2+}$ (Me$_2$phen = 4,7-dimethyl-1,10-phenanthroline) in the presence of Sc^{3+} in water under visible light irradiation.[102] The photocatalytic cycle for H$_2$O$_2$ production is shown in Scheme 8, where photoreduction of O$_2$ by [Ru^{II}(Me$_2$phen)$_3$]$^{2+}$ in the presence of Sc^{3+} is combined with the catalytic oxidation of water by [Ru^{III}(Me$_2$phen)$_3$]$^{3+}$.[103] Photoinduced electron transfer from the excited state of [Ru^{II}(Me$_2$phen)$_3$]$^{2+}$ to O$_2$ results in the formation of [Ru^{III}(Me$_2$phen)$_3$]$^{3+}$ and O$_2$$^{\bullet-}$ that binds to Sc^{3+} and the disproportionation of O$_2$$^{\bullet-}$–Sc^{3+} in water yields H$_2$O$_2$.[104] Four equivalents of [Ru^{III}(Me$_2$phen)$_3$]$^{3+}$ can oxidize H$_2$O to O$_2$ in the presence of a WOC.[102,103]
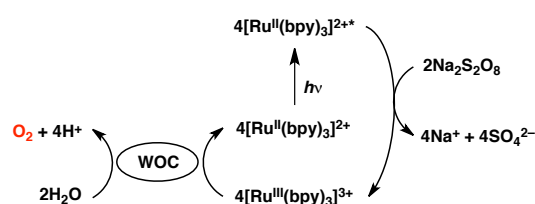
Scheme 8. Catalytic cycle for photocatalytic water oxidation by persulfate with [Ru^{II}(Me$_2$phen)$_3$]$^{2+}$ and WOC in the presence of Sc^{3+} in water.

The time course of the photocatalytic production of H$_2$O$_2$ with [Ru^{II}(Me$_2$phen)$_3$]$^{2+}$ and [Ir(Cp*)(H$_2$O)$_3$]$^{2+}$ in the presence of Sc(NO$_3$)$_3$ (100 mM) in water at various temperatures is shown in Figure 4, where an induction period is observed in particular at 278 K.[102] The rate of formation of H$_2$O$_2$ increased rapidly after the induction period.[102] Such a sigmoidal behavior in the initial
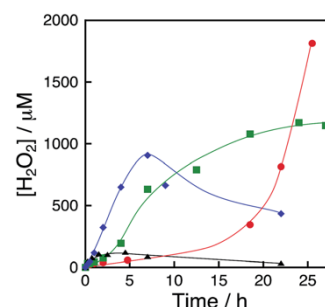
Figure 4. Time courses of H$_2$O$_2$ production under visible light (λ > 420nm) irradiation of [Ru^{II}(Me$_2$phen)$_3$]$^{2+}$ (20 µM) in the presence of [Ir(Cp*)(H$_2$O)$_3$]$^{2+}$ (100 µM) and Sc^{3+} (100 mM) in an O$_2$-saturated aqueous solution (3.0 mL) at 333 K (black triangles), 313 K (blue diamonds), 293 K (green squares) and 278 K (red circles).

stage of H$_2$O$_2$ production with [Ir(Cp*)(H$_2$O)$_3$]$^{2+}$ (red in Figure 4) indicates that [Ir(Cp*)(H$_2$O)$_3$]$^{2+}$ acts as a precatalyst to produce catalytically more active nanoparticles during the photocatalytic production of H$_2$O$_2$.[102] The initial rate of H$_2$O$_2$ production increases with increasing temperature, but the maximum H$_2$O$_2$ concentration decreased because of the enhanced decomposition of H$_2$O$_2$ (Figure 4).[102] The formation of nanoparticles was confirmed by DLS measurements. The size of nanoparticles formed after 12 h photoirradiation at 278 K was 21 nm, whereas the size increased to 240 nm after 36 h photoirradiation.[102] Large-sized particles (450 nm) were obtained after 12 h photoirradiation at 333 K.[102] Thus, the size of the particles depends on the photoirradiation time and temperature. XPS measurements of the nanoparticles centrifugally recovered from the reaction solution after the H$_2$O$_2$ production reaction indicated that the formed nanoparticles were composed of Ir(OH)$_3$ as the case of water oxidation by CAN (vide supra).[80,102]

Heterogeneous Catalysts

Metal oxides, in the form of dispersed powders, have been extensively examined as heterogeneous WOCs in the photocatalytic oxidation of water by persulfate with [Ru(bpy)$_3$]$^{2+}$ (Scheme 2).[104-122] The yields of O$_2$ and the catalytic reactivity in the catalytic oxidation of water by persulfate with heterogeneous catalysts are listed in Table 3.[106-122] The most efficient metal oxide catalyst is IrO$_2$, which gave >99% yield of O$_2$ per persulfate and a rate of O$_2$ formation of 190 µM s^{-1} g^{-1}.[106,107] IrO$_2$ nanocrystals were reported to photocatalyze oxygen formation from aqueous solutions of sacrificial electron acceptors, without the use of an external light absorber such as [Ru(bpy)$_3$]$^{2+}$.[108] Photochemical charge carriers are formed when electrons are excited from the Ir-d(t$_{2g}$) to the Ir-d(e$_g$) band (1.5-2.75 eV) or from the O-p to the Ir-d(e$_g$) band (>3.0 eV).[108] The O$_2$ yield in the photocatalytic oxidation of water by persulfate with IrO$_2$ nanoparticles was 73%, which is smaller than the case with [Ru(bpy)$_3$]$^{2+}$ (>99%) in Table 3.[108] The rate of O$_2$ formation by persulfate with [Ru(bpy)$_3$]$^{2+}$ (190 µM s^{-1} g^{-1}) in Table 3.[108]

Table 3. TON and yield in photocatalytic oxidation of water by persulfate using heterogeneous catalysts.

Catalyst	pH	Rate[a]	Yield (%)[b]	Ref
IrO$_2$	5.4[c]	190	>99	106
IrO$_2$[d]	10	18	73	108
RuO$_2$	5.0	-	27	109
RuO$_2$ NP[e]	5.4	-	95	110
RuO$_x$/Y-zeolite[f]		-	31	111
NiFe$_2$O$_4$[g]	8.0	2.7	74	112
Co$_3$O$_4$[g]	8.0	2.4	64	112
Co$_3$O$_4$-150[h]	7.0	-	27	113
Co$_3$O$_4$-750[h]	7.0	-	16	113
NiO[g]	8.0	1.5	52	112
α-NiO nanorods[i]	8.5	1.8	44	114
Fe$_3$O$_4$[g]	9.0	0.95	55	112
Fe$_2$O$_3$[g]	8.5	0.65	24	112
Fe$_2$O$_3$ (nanocubes)	8.0	-	13.4	115
Fe$_2$O$_3$ (nanoplates)	8.0	-	4.5	115
Fe$_2$O$_3$ (nanoflakes)	8.0	-	3.0	115
Fe$_2$O$_3$ (nanoarticle)	8.0	-	17.7	115
CuFe$_2$O$_4$	8.5	11	73	116
LaCoO$_3$	7.0	5.5	74	117
CoWO$_4$[j]	7.0	1.3	19	117
La$_{0.7}$Sr$_{0.3}$CoO$_3$[j]	7.0	3.6	59	117
NdCoO$_3$[j]	7.0	4.6	59	117
YCoO$_3$[j]	7.0	1.8	24	117
CoNCN[k]	9.0	-	76	118
NiMnO$_3$	7.0	9.6	52	119
α-MnO$_2$	7.0	5.0	24	119
Mn$_2$O$_3$	7.0	2.5	18	119
Mn$_2$O$_3$ (bixbyite)	7.0	2.4	-	120
Mn$_3$O$_4$	7.0	1.0	4	119
Mn$_3$O$_4$ ((hausmannite)	7.0	1.0	-	120
γ-MnO$_2$	7.0	0.94	-	120
NiO/CoO/Fe$_2$O$_3$	8.5	-	64	121
NiO + CoO + Fe$_2$O$_3$	8.5	-	47	121
[Co^{II}(H$_2$O)$_{1.79}$]$_{1.42}$[(Co$^{III}_{0.85}$Pt$^{IV}_{0.15}$)(CN)$_6$]	8.0	62	100	125

[a] O$_2$ evolution rate: mM s^{-1} g^{-1} (catalyst weight: g). [b] Yield is defined as twice the number of moles of O$_2$ per mole of Na$_2$S$_2$O$_8$. [c] 5.0 × 10^{-2} M (1.0:1.3) Na$_2$SiF$_6$-NaHCO$_3$ buffer. [d] Photoirradiation (300 W Xe lamp, λ > 400 nm) of a buffer solution (100 mL, pH 10) containing Na$_2$S$_2$O$_8$ (42.9 μmol) and IrO$_2$ (3.7 mg). [e] RuO$_2$ supported on mesoporous silica SBA-15. [f] Obtained starting from zeolite Y and Ru$_3$(CO)$_{12}$. [g] Photoirradiation (λ > 420 nm) of an aqueous buffer solution (pH 8.0, 2.0 mL) containing the catalyst (0.50 g L^{-1}), Na$_2$S$_2$O$_8$ (5.0 mM), and [Ru(bpy)$_3$]$^{2+}$ (0.25 mM). [h] The number denotes the calcination temperature. [i] α-NiO nanowires and α-NiO nanoplates exhibited similar catalytic reactivity. [j] Photoirradiation (Xe lamp, λ > 420 nm) of a phosphate buffer solution (50 mM, 2.0 mL, pH 7.0) containing the catalyst (0.25 g L^{-1}), Na$_2$S$_2$O$_8$ (5.0 mM), and [Ru(bpy)$_3$]$^{2+}$ (0.25 mM). [k] cobalt carbodiimide.
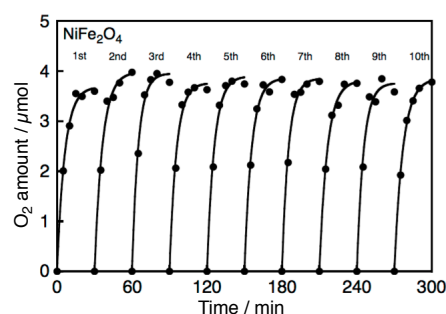

Figure 5. Time courses of O$_2$ evolution under photoirradiation (Xe lamp, λ > 420 nm) of a phosphate buffer solution (pH 8.0, 2.0 mL) containing Na$_2$S$_2$O$_8$ (5.0 mM) and [Ru(bpy)$_3$]SO$_4$ (0.25 mM) with NiFe$_2$O$_4$ (0.50 g L^{-1}) at room temperature in 10 repetitive examinations.

RuO$_2$ supported on mesoporous silica SBA-15 (RuO$_2$ NP) acted as an efficient WOC in the photocatalytic oxidation of water by persulfate with [Ru(bpy)$_3$]$^{2+}$ to afford 95% yield of O$_2$,[110] which is much higher than RuO$_2$ (27%)[109] and RuO$_2$/Y-zeolite-based catalysts (31%).[111] The quantum efficiency (twice of the quantum yield) was determined to be 11.3%.[110] RuO$_2$ NP has been recycled up to five times with minimal loss of activity.[110]

Among earth-abundant metal oxides WOCs, NiFe$_2$O$_4$ exhibited the highest catalytic activity to afford 73% yield of O$_2$, which is higher than those of cobalt oxides, iron oxides, and nickel oxides (Table 3).[112-115] NiFe$_2$O$_4$ can be easily collected from the solution after the reaction because of its ferromagnetic properties.[112] The high O$_2$ yield with NiFe$_2$O$_4$ was maintained even after the 10th run in 5 h (Figure 5). No significant change in either the powder X-ray diffraction (PXRD) pattern or the morphology of the NiFe$_2$O$_4$ catalyst was observed after the water oxidation reaction.[112] Cyclic voltammetry studies of electrocatalytic water oxidation with NiFe$_2$O$_4$ suggested that a high-valent nickel species may be the active species for the photocatalytic water oxidation.[112]

The initial rate of H$_2$O$_2$ production with NiFe$_2$O$_4$ nanoparticles with diameters of 120 nm and 91 nm was accelerated 22 times and 33 times, respectively, as compared to the as-prepared NiFe$_2$O$_4$ with diameter of 1300 nm (Figure 6).[102] This increase in reactivity results from an increase in the surface area with decreasing the diameter size. The linear relationship between the initial rates of H$_2$O$_2$ production and the surface areas of NiFe$_2$O$_4$ nanoparticles indicates that the reactivity of each active site for water oxidation in the surface of NiFe$_2$O$_4$ remains unchanged irrespective of the particle size.[102]

In order to reuse the nanoparticles after H$_2$O$_2$ production ceased, an aliquot of an aqueous solution containing a high concentration of [Ru^{II}(Me$_2$phen)$_3$]$^{2+}$ was added to the reaction suspension repeatedly, in which the amount of [Ru^{II}(Me$_2$phen)$_3$]$^{2+}$ added to the starting suspension at each run was calculated in terms of the concentration increase of 200 μM. The concentration of H$_2$O$_2$ in the resulting suspension increased to be as high as 3.3 mM, ensuring the high stability of the
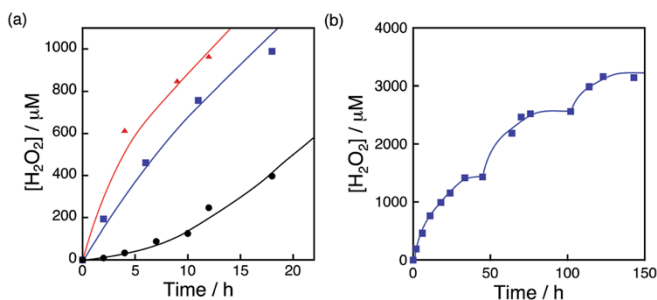
Figure 6. (a) Time courses of H_2O_2 production under visible light irradiation (λ > 420 nm) of $[Ru^{II}(Me_2phen)_3]^{2+}$ (200 μM) in the presence of Sc^{3+} (100 mM) and $NiFe_2O_4$ (0.17 g L^{-1}) with diameters of 1300 nm (black circles), 120 nm (blue squares) and 91 nm (red triangles) in O_2-saturated H_2O (3.0 mL, $[O_2]$ = 1.2 mM). (b) Time course of H_2O_2 production in the presence of $NiFe_2O_4$ (0.17 g L^{-1}) and Sc^{3+} (100 mM) under visible light irradiation (λ > 420 nm) of $[Ru^{II}(Me_2phen)_3]^{2+}$ (200 μM) in O_2-saturated H_2O (3.0 mL, $[O_2]$ = 1.2 mM). $[Ru^{II}(Me_2phen)_3]^{2+}$ was added twice to the reaction suspension at 50 h and 100 h during photoirradiation. The amount of $[Ru^{II}(Me_2phen)_3]^{2+}$ added each time at 50 h and 100 h to the reaction suspension was calculated in terms of the concentration increase of 200 μM.

nanoparticles as WOCs (Figure 6b).[102]

CuFe$_2$O$_4$ nanocrystals with cubic jacobsite structure also exhibited high catalytic activity in the photocatalytic water oxidation by persulfate with $[Ru(bpy)_3]^{2+}$ to afford 73% O_2 yield (Table 3). As in the case of $NiFe_2O_4$ (vide supra), $CuFe_2O_4$ can be easily separated from reaction solution by magnetic separation while maintaining excellent water oxidation activity in the fourth and fifth runs.[116] The catalytic activity of cobalt-containing metal oxides, such as perovskites ($LaCoO_3$, $NdCoO_3$, $YCoO_3$, $La_{0.7}Sr_{0.3}CoO_3$), spinel (Co_3O_4) and wolframite ($CoWO_4$), was compared in the photocatalytic water oxidation by persulfate with $[Ru(bpy)_3]^{2+}$ (Table 3).[117] The catalysts with the perovskite structure exhibited higher catalytic activity as compared with those of the spinel and wolframite structures.[117] Among them, $LaCoO_3$ acts as the best catalyst to afford the highest O_2 yield (74%).[117] Ni^{2+} ion doped manganese oxide ($NiMnO_3$) also exhibited high catalytic activity in the photocatalytic water oxidation by persulfate with $[Ru(bpy)_3]^{2+}$ to yield 52% O_2 yield as compared with manganese oxides.[119,120]

Recently, coordination polymers emerged as potential candidates, possessing both designable structures at the atomic level and robustness under harsh reaction conditions.[122,123] Heteropolynuclear cyanide complexes are the simplest class of coordination polymers. In general, heteropolynuclear cyanide complexes have a cubic structure as far as the contained metal ions allow octahedral coordination.[124] Heteropolynuclear cyanide complexes can be easily modified as heterogeneous catalysts suitable for water oxidation. A series of the heteropolynuclear cyanide complexes containing Pt^{IV} ions, $[Co^{II}(H_2O)_m]_n[(Co^{III}_{1-x}Pt^{IV}_x)(CN)_6]$, were prepared by mixing an aqueous solution containing both $K_3[Co^{III}(CN)_6]$ and $K_2[Pt^{IV}(CN)_6]$ with various Co^{III}/Pt^{IV} ratios ranging from 1:0 to 0:1, and an aqueous solution containing an excess amount of $Co(NO_3)_2$.[125]

Powder X-ray diffraction patterns for the heteropolynuclear cyanide complexes with the Pt^{IV} ion content ranging from 0 to 1
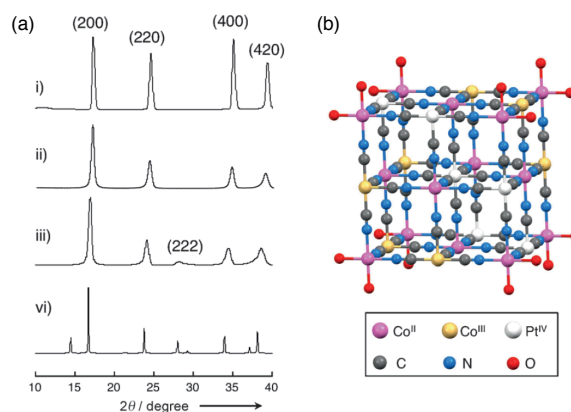
Figure 7. (a) Powder X-ray diffraction patterns of a series of heteropolynuclear cyanide complexes, $[Co^{II}(H_2O)_m]_n[Co^{III}_{1-x}Pt^{IV}_x(CN)_6]$; i) x=0, ii) x=0.15, iii) x=0.43, and iv) x=1. (b) A schematic drawing of $[Co^{II}(H_2O)_m]_n[Co^{III}_{1-x}Pt^{IV}_x(CN)_6]$. Hydrogen atoms of water molecules are omitted.

(Figure 7a) were assigned as a cubic structure (Figure 7b), which is often called as Prussian blue. The gradual decrease of the diffraction peaks in the 2θ angle in accordance with the increase in the Pt^{IV} ion content and reflects the expansion of a unit cell resulting from the larger ionic radii of a Pt^{IV} ion (0.77 Å) relative to that of a Co^{III} ion (0.69 Å).[126]

The stoichiometric amount of O_2 (100%) was obtained in the photocatalytic oxidation by persulfate with $[Ru(bpy)_3]^{2+}$ using $[Co^{II}(H_2O)_{1.79}]_{1.42}[(Co^{III}_{0.85}Pt^{IV}_{0.15})(CN)_6]$ (x = 0.15) as a WOC at pH 8.0.[125] The initial O_2 evolution rate increases with an increase in the Pt^{IV} ion content in $[Co^{II}(H_2O)_m]_n[(Co^{III}_{1-x}Pt^{IV}_x)(CN)_6]$ to reach the maximum using $[Co^{II}(H_2O)_{1.79}]_{1.42}[(Co^{III}_{0.85}Pt^{IV}_{0.15})(CN)_6]$ as a WOC at the rate exceeded 10 nmol s^{-1}, which is comparable to that reported for most active IrO_2 nanoparticles.[125] Thus, the addition of $Pt^{IV}(CN)_6^{2-}$ units to cobalt cyanide complexes enhanced the catalytic activity for water oxidation by increasing the oxidation potential of N-bound Co^{II} ions acting as active sites through electronic and structural modifications.[125]

5. Conclusion

Homogeneous WOCs in the photocatalytic oxidation of water by persulfate ($Na_2S_2O_8$) with $[Ru(bpy)_3]^{2+}$ provided valuable insights into the catalytic mechanisms, including intermediates such as metal-oxo and dinuclear metal-peroxo complexes. The nucleophilic attack of water to metal-oxo species or radical coupling of metal-oxo species for the O-O bond formation is determined depending on the types of metals and ligands. Ligands of metal complexes are often oxidized during the photocatalytic water oxidation and metal complexes are converted to the catalytically more active nanoparticles which are composed of metal oxides and hydroxides. The size of nanoparticles is determined by the ligands and water reaction conditions such as pH and temperature. Whether metal complexes remain homogeneous or they are converted to heterogeneous nanoparticles is also determined by the type of metals, ligands and water oxidation conditions in particular by

pH. Among heterogeneous WOCs, heteropolynuclear cyanide complexes serve as good candidates for development of more efficient WOCs to afford 100% of O_2, because the structure and electronic states of heteropolynuclear cyanide complexes can be easily modified as compared with metal oxides or hydroxide nanoparticles. This focused review is hoped to help better understanding of catalysis of homogeneous and heterogeneous WOC and their combinations in water oxidation reactions.

[1] E. W. McFarland, *Energy Environ. Sci.* **2014**, *7*, 846-854.
[2] T. A. Faunce, W. Lubitz, A. W. (Bill) Rutherford, D. MacFarlane, G. F. Moore, P. Yang, D. G. Nocera, T. A. Moore, D. H. Gregory, S. Fukuzumi, K. B. Yoon, F. A. Armstrong, M. R. Wasielewski, S. Styring, *Energy Environ. Sci.* **2013**, *6*, 695-698.
[3] N. S. Lewis, D. G. Nocera, *Proc. Natl. Acad. Sci. U.S.A.* **2006**, *103*, 15729-15735.
[4] D. Kim, K. K. Sakimoto, D. Hong, P. Yang, *Angew. Chem. Int. Ed.* **2015**, *54*, 3259-3266.
[5] S. Fukuzumi, K. Ohkubo, T. Suenobu, *Acc. Chem. Res.* **2014**, *47*, 1455-1464.
[6] S. Fukuzumi, K. Ohkubo, *J. Mater. Chem.* **2012**, *22*, 4575-4587.
[7] D. Gust, T. A. Moore, A. L. Moore, *Acc. Chem. Res.* **2009**, *42*, 1890-1898.
[8] S. Fukuzumi, *Phys. Chem. Chem. Phys.* **2008**, *10*, 2283-2297.
[9] M. R. Wasielewski, *Acc. Chem. Res.* **2009**, *42*, 1910−1921.
[10] S. Fukuzumi, T. Kojima, *J. Mater. Chem.* **2008**, *18*, 1427−1439.
[11] G. Knör, *Coord. Chem. Rev.* **2015**, *304-305*, 102-108.
[12] S. Fukuzumi, *Curr. Opin. Chem. Biol.* **2015**, *25*, 18-26.
[13] S. Berardi, S. Drouet, L. Francàs, C. Gimbert-Suriñach, M. Guttentag, C. Richmond, T. Stoll, A. Llobet, *Chem. Soc. Rev.* **2014**, *43*, 7501-7519.
[14] S. Fukuzumi, *Biochim. Biophys. Acta* **2015**, in press.
[15] J. R. McKone, N. S. Lewis, H. B. Gray, *Chem. Mater.* **2014**, *26*, 407-414.
[16] S. Fukuzumi, Y. Yamada, *Aust. J. Chem.* **2014**, *67*, 354-364.
[17] J. Ran, J. Zhang, J. Yu, M. Jaroniec, S. Z. Qiao, *Chem. Soc. Rev.* **2014**, *43*, 7787-7812.
[18] S. Fukuzumi, Y. Yamada, *ChemSusChem* **2013**, *6*, 1834-1847.
[19] S. Fukuzumi, K. Ohkubo, *Dalton Trans.* **2013**, *42*, 15846-15858.
[20] T. Grewe, M. Meggouh, H. Tueysuez, *Chem. Asian J.* **2015**, in press.
[21] S. Fukuzumi, *Eur. J. Inorg. Chem.* **2008**, 1351-1362.
[22] X. Zou, Y. Zhang, *Chem. Soc. Rev.* **2015**, *44*, 5148-5180.
[23] S. Fukuzumi, *Bull. Chem. Soc. Jpn.* **2006**, *79*, 177-195.
[24] M. Suga, F. Akita, K. Hirata, G. Ueno, H. Murakami, Y. Nakajima, T. Shimizu, K. Yamashita, M. Yamamoto, H. Ago, J.-R. Shen, *Nature* **2015**, *517*, 99-103.
[25] Y. Umena, K. Kawakami, J.-R. Shen, N. Kamiya, *Nature* **2011**, *473*, 55-60.
[26] J. Yano, V. Yachandra, *Chem. Rev.* **2014**, *114*, 4175-4205.
[27] N. Cox, D. A. Pantazis, F. Neese, W. Lubitz, *Acc. Chem. Res.* **2013**, *46*, 1588-1596.
[28] M. D. Kärkäs, O. Verho, E. V. Johnston, B. Åkermark, *Chem. Rev.* **2014**, *114*, 11863-12001.
[29] L. Duan, L. Wang, F. Li, F. Li, L. Sun, *Acc. Chem. Res.* **2015**, *48*, 2084-2096.
[30] M. M. Najafpour, M. Z. Ghobadi, B. Haghighi, T. Tomo, J.-R. Shen, S. I. Allakhverdiev, *Biochim. Biophys. Acta* **2015**, *1847*, 294-306.
[31] A. R. Parent, R. H. Crabtree, G. W. Brudvig, *Chem. Soc. Rev.* **2013**, *42*, 2247-2252.
[32] K. J. Young, B. J. Brennan, R. Tagore, G. W. Brudvig, *Acc. Chem. Res.* **2015**, *48*, 567-574.
[33] K. J. Young, L. A. Martini, R. L. Milot, R. C. Snoeberger III, V. S. Batista, C. A. Schmuttenmaer, R. H. Crabtree, G. W. Brudvig, *Coord. Chem. Rev.* **2012**, *256*, 2503-2520.
[34] S. Fukuzumi, D. Hong, Y. Yamada, *J. Phys. Chem. Lett.* **2013**, *4*, 3458-3467.
[35] X. Wu, F. Lia, B. Zhanga, L. Sun, *J. Photochem. Photobiol. C: Photochem. Rev.* **2015**, in press.
[36] S. Fukuzumi, Y. Yamada, *J. Mater. Chem.* **2012**, *22*, 24284-24296.
[37] D. G. H. Hetterscheid, J. N. H. Reek, *Angew. Chem. Int. Ed.* **2012**, *51*, 9740-9747.
[38] D. J. Wasylenko, R. D. Palmer, C. P. Berlinguette, *Chem. Commun.* **2013**, *49*, 218-227.
[39] A. Sartorel, M. Bonchio, S. Campagna, F. Scandola, *Chem. Soc. Rev.* **2013**, *42*, 2262-2280.
[40] A. Lewandowska-Andralojc, D. E. Polyansky, *J. Phys. Chem. A* **2013**, *117*, 10311-10319.
[41] X. Du, Y. Ding, F. Song, B. Ma, J. Zhao, J. Song, *Chem. Commun.* **2015**, *51*, 13925-13928.
[42] F. Evangelisti, R. Moré, F. Hodel, S. Luber, G. R. Patzke, *J. Am. Chem. Soc.* **2015**, *137*, 11076-11084.
[43] F. Evangelisti, R. Güttinger, R. Moré, S. Luber, G. R. Patzke, *J. Am. Chem. Soc.* **2013**, *135*, 18734-18737.
[44] J. Wei, Y. Feng, P. Zhou, Y. Liu, J. Xu, R. Xiang, Y. Ding, C. Zhao, L. Fan, C. Hu, *ChemSusChem* **2015**, *8*, 2630-2634.
[45] Y. V. Geletii, Z. Huang, Y. Hou, D. G. Musaev, T. Lian, C. L. Hill, *J. Am. Chem. Soc.* **2009**, *131*, 7522-7523.
[46] X.-B. Han, Y.-G. Li, Z.-M. Zhang, H.-Q. Tan, Y. Lu, E.-B. Wang, *J. Am. Chem. Soc.* **2015**, *137*, 5486−5493.
[47] X.-B. Han, Z.-M. Zhang, T. Zhang, Y.-G. Li, W. Lin, W. You, Z.-M. Su, E.-B. Wang, *J. Am. Chem. Soc.* **2014**, *136*, 5359-5366.
[48] H. Lv, J. Song, Y. V. Geletii, J. W. Vickers, J. M. Sumliner, D. G. Musaev, P. Kögerler, P. F. Zhuk, J. Bacsa, G. Zhu, C. L. Hill, *J. Am. Chem. Soc.* **2014**, *136*, 9268-9271.
[49] T. Zhou, D. Wang, S.-C.-K. Goh, J. Hong, J. Han, J. Mao, R. Xu, *Energy Environ. Sci.* **2015**, *8*, 526-534.
[50] R. Al-Oweini, A. Sartorel, B. S. Bassil, M. Natali, S. Berardi, F. Scandola, U. Kortz, M. Bonchio, *Angew. Chem. Int. Ed.* **2014**, *53*, 11182-11185.
[51] R. Xiang, Y. Ding, J. Zhao, *Chem. Asian J.* **2014**, *9*, 3228-3237.
[52] C. Besson, Z. Huang, Y. V. Geletii, S. Lense, K. I. Hardcastle, D. G. Musaev, T. Lian, A. Proust, C. L. Hill, *Chem. Commun.* **2010**, *46*, 2784-2786.
[53] S. Tanaka, M. Annaka, K. Sakai, *Chem. Commun.* **2012**, *48*, 1653-1655.
[54] B. Das, A. Orthaber, S. Ott, A. Thapper, *Chem. Commun.* **2015**, *51*, 13074-13077.
[55] M. Chen, S.-M. Ng, S.-M. Yiu, K.-C. Lau, R. J. Zeng. T.-C. Lau, *Chem. Commun.* **2014**, *50*, 14956-14959.
[56] T. Nakazono, A. R. Parent, K. Sakai, *Chem. Commun.* **2013**, *49*, 6325-6327.

[57] T. Nakazono, A. R. Parent, K. Sakai, *Chem. Eur. J.* **2015**, *21*, 6723-6726.

[58] C.-F. Leung, S.-M. Ng, C.-C. Ko, W.-L. Man, J. Wu, L. Chen, T.-C. Lau, *Energy Environ. Sci.* **2012**, *5*, 7903-7907.

[59] H. Li, F. Li, B. Zhang, X. Zhou, F. Yu, L. Sun, *J. Am. Chem. Soc.* **2015**, *137*, 4332-4335.

[60] L. Wang, L. Duan, L. Tong, L. Sun, *J. Catal.* **2013**, *306*, 129-132.

[61] L. Wang, M. Mirmohades, A. Brown, L. Duan, F. Li, Q. Daniel, R. Lomoth, L. Sun, L. Hammarström, *Inorg. Chem.* **2015**, *54*, 2742-2751.

[62] A. Lewandowska-Andralojc, D. E. Polyansky, R. Zong, R. P. Thummel, E. Fujita, *Phys. Chem. Chem. Phys.* **2013**, *15*, 14058-14068.

[63] C. Panda, J. Debgupta, D. D. Díaz, K. K. Singh, S. S. Gupta, B. B. Dhar, *J. Am. Chem. Soc.* **2014**, *136*, 12273-12282.

[64] M.-P. Santoni, G. L. Ganga, V. M. Nardo, M. Natali, F. Puntoriero, F. Scandola, S. Campagna, *J. Am. Chem. Soc.* **2014**, *136*, 8189-8192.

[65] S. Berardi, L. Francàs, S. Neudeck, S. Maji, J. Benet-Buchholz, F. Meyer, A. Llobet, *ChemSusChem* **2015**, *8*, 3688-3696.

[66] T. Ishizuka, A. Watanabe, H. Kotani, D. Satonaka, D. Hong, T. Wada, Y. Shiota, K. Yoshizawa, K. Ohara, K. Yamaguchi, S. Kato, Shunichi Fukuzumi, T. Kojima, submitted.

[67] Y. V. Geletii, B. Botar, P. Kögerler, D. A. Hillesheim, D. G. Musaev, C. L. Hill, *Angew. Chem. Int. Ed.* **2008**, *47*, 3896-3899.

[68] A. Sartorel, M. Carraro, G. Scorrano, R. D. Zorzi, S. Geremia, N. D. McDaniel, S. Bernhard, M. Bonchio, *J. Am. Chem. Soc.* **2008**, *130*, 5006-5007.

[69] Q. Yin, J. M. Tan, C. Besson, Y. V. Geletii, D. G. Musaev, A. E. Kuznetsov, Z. Luo, K. I. Hardcastle, C. L. Hill, *Science* **2010**, *328*, 342-345.

[70] S. Bang, Y.-M. Lee, S. Hong, K.-B. Cho, Y. Nishida, M. S. Seo, R. Sarangi, S. Fukuzumi, W. Nam, *Nat. Chem.* **2014**, *6*, 934-940.

[71] S. Fukuzumi, K. Ohkubo, Y.-M. Lee, W. Nam, *Chem. Eur. J.* **2015**, *21*, 17548-17559.

[72] M. Murakami, D. Hong, T. Suenobu, S. Fukuzumi, *J. Am. Chem. Soc.* **2011**, *133*, 11605-11613.

[73] D. K. Dogutan, R. McGuire, Jr., D. G. Nocera, *J. Am. Chem. Soc.* **2011**, *133*, 9178-9180.

[74] D. J. Wasylenko, R. D. Palmer, E. Schott, C. P. Berlinguette, *Chem. Commun.* **2012**, *48*, 2107-2109.

[75] D. Wang, J. T. Groves, *Proc. Natl. Acad. Sci. USA* **2013**, *110*, 15579-15584.

[76] L. Wang, L. Duan, Y. Wang, M. S. G. Ahlquist, L. Sun, *Chem. Commun.* **2014**, *50*, 12947-12950.

[77] S. Neudeck, S. Maji, I. López, S. Meyer, F. Meyer, A. Llobet, *J. Am. Chem. Soc.* 2014, *136*, 24-27.

[78] F. Bozoglian, S. Romain, M. Z. Ertem, T. K. Todorova, C. Sens, J. Mola, M. Rodríguez, I. Romero, J. Benet-Buchholz, X. Fontrodona, C. J. Cramer, L. Gagliardi, A. Llobet, *J. Am. Chem. Soc.* **2009**, *131*, 15176-15187.

[79] X. Sala, S. Maji, R. Bofill, J. García-Antón, L. Escriche, A. Llobet, *Acc. Chem. Res.* **2014**, *47*, 504-516.

[80] D. Hong, M. Murakami, Y. Yamada, S. Fukuzumi, *Energy Environ. Sci.* **2012**, *5*, 5708-5716.

[81] S. Fukuzumi, D. Hong, *Eur. J. Inorg. Chem.* **2014**, 645-659.

[82] J. J. Stracke. R. G. Finke, *ACS Catal.* **2014**, *4*, 909-933.

[83] M. A. Asraf, H. A. Younus, M. Yusubov, Francis Verpoort, *Catal. Sci. Technol.* **2015**, *5*, 4901-4925.

[84] J. J. Stracke, R. G. Finke, *ACS Catal.* **2014**, *4*, 79-89.

[85] J. J. Stracke, R. G. Finke, *ACS Catal.* **2013**, *3*, 1209-1219.

[86] S. Goberna-Ferrón, J. Soriano-López, J. R. Galán-Mascarós, M. Nyman, *Eur. J. Inorg. Chem.* **2015**, *17*, 2833-2840.

[87] S. Goberna-Ferrón, L. Vigara, J. Soriano-López, J. R. Galán-Mascarós, *Inorg. Chem.* **2012**, *51*, 11707-11715.

[88] J. Soriano-López, S. Goberna-Ferrón, L. Vigara, J. J. Carbó, J. M. Poblet, J. R. Galán-Mascarós, *Inorg. Chem.* **2013**, *52*, 4753-4755.

[89] J. W. Vickers, H. Lv, J. M. Sumliner, G. Zhu, Z. Luo, D. G. Musaev, Y. V. Geletii, C. L. Hill, *J. Am. Chem. Soc.* **2013**, *135*, 14110-14118.

[90] Y.-H. Lai, C.-Y. Lin, Y. Lv, T. C. King, A. Steiner, N. M. Muresan, L. Gan, D. S. Wright, E. Reisner, *Chem. Commun.* **2013**, *49*, 4331-4333.

[91] A. Savini, A. Bucci, G. Bellachioma, L. Rocchigiani, C. Zuccaccia, A. Llobet, A. Macchioni, *Eur. J. Inorg. Chem.* **2014**, 690-697.

[92] M. M. Najafpour, F. Ebrahimi, R. Safdari, M. Z. Ghobadi, M. Tavahodi, P. Rafighi, *Dalton Trans.* **2015**, *44*, 15435-15440.

[93] J. M. Thomsen, D. L. Huang, R. H. Crabtree, G. W. Brudvig, *Dalton Trans.* **2015**, *44*, 12452-12472.

[94] D. Hong, J. Jung, J. Park, Y. Yamada, T. Suenobu, Y.-M. Lee, W. Nam, S. Fukuzumi, *Energy Environ. Sci.* **2012**, *5*, 7606-7616.

[95] S. Fu, Y, Liu, Y. Ding, X. Du, F. Song, R. Xiang, B. Ma, *Chem. Commun.* **2014**, *50*, 2167-2169.

[96] H. Chen, Z. Sun, X. Liu, A. Han, P. Du, *J. Phys. Chem. C* **2015**, *119*, 8998-9004.

[97] G. Chen, L. Chen, S.-M. Ng, W.-L. Man, T.-C. Lau, *Angew. Chem. Int. Ed.* **2013**, *52*, 1789-1791.

[98] D. Hong, S. Mandal, Y. Yamada, Y.-M. Lee, W. Nam, A. Llobet, S. Fukuzumi, *Inorg. Chem.* **2013**, *52*, 9522-9531.

[99] H. Liu, M. Schilling, M. Yulikov, S. Luber, G. R. Patzke, *ACS Catal.* **2015**, *5*, 4994-4999.

[100] G. Chen, L. Chen, S.-M. Ng, T.-C. Lau, *ChemSusChem* **2014**, *7*, 127-134.

[101] A. Singh, S. L. Y. Chang, R. K. Hocking, U. Bach, L. Spiccia, *Energy Environ. Sci.* **2013**, *6*, 579-586.

[102] Y. Isaka, S. Kato, D. Hong, T. Suenobu, Y. Yamada, S. Fukuzumi, *J. Mater. Chem. A* **2015**, *3*, 12404-12412.

[103] S. Kato, J. Jung, T. Suenobu, S. Fukuzumi, *Energy Environ. Sci.* **2013**, *6*, 3756-3764.

[104] A. Harriman, I. J. Pickering, J. M. Thomas, *J. Chem. Soc, Faraday Trans. 1* **1988**, *84*, 2795-2806.

[105] A. Harriman, *Eur. J. Inorg. Chem.* **2014**, 573-580.

[106] M. Hara, C. C. Waraksa, J. T. Lean, B. A. Lewis, T. E. Mallouk, *J. Phys. Chem. A* **2000**, *104*, 5275-5280.

[107] M. Hara, J. T. Lean, T. E. Mallouk, *Chem. Mater.* **2001**, *13*, 4668-4675.

[108] F. A. Frame, T. K. Townsend, R. L. Chamousis, E. M. Sabio, T. Dittrich, N. D. Browning, F. E. Osterloh, *J. Am. Chem. Soc.* **2011**, *133*, 7264-7267.

[109] A. Harriman, M.-C. Richoux, P. A. Christensen, S. Mosseri, P. Neta, *J. Chem. Soc., Faraday Trans. 1* **1987**, *83*, 3001-3014.

[110] Y. Zhang, E. C. Judkins, D. R. McMillin, D. Mehta, T. Ren, *ACS Catal.* **2013**, *3*, 2474-2478.

[111] S. K. Das, P. K. Dutta, *Microporous Mesoporous Mater.* **1998**, *22*, 475-483.

[112] D. Hong, Y. Yamada, T. Nagatomi, Y. Takai, S. Fukuzumi, *J. Am. Chem. Soc.* **2012**, *134*, 19572-19575.

[113] X. Deng, H.-J. Bongard, C. K. Chan, H. Tüysüz, *CheSusChem* **2015**, in press.

[114] X. Du, Y. Ding, C. Li, *ChemCatChem* **2015**, *7*, 2370-2376.

[115] Q. Xiang, G. Chen, T.-C. Lau, *RSC Adv.* **2015**, *5*, 52210-52216.

[116] X. Du, Y. Ding, R. Xiang, X. Xiang, *Phys. Chem. Chem. Phys.* **2015**, *17*, 10648-10655.

[117] Y. Yamada, K. Yano, D. Hong, S. Fukuzumi, *Phys. Chem. Chem. Phys.* **2012**, *14*, 5753-5760.

[118] D. Ressnig, M. Shalom, J. Patscheider, R. Moré, F. Evangelisti, M. Antonietti, G. R. Patzke, *J. Mater. Chem. A* **2015**, *3*, 5072-5082.

[119] D. Hong, Y. Yamada, A. Nomura, S. Fukuzumi, *Phys. Chem. Chem. Phys.* **2013**,*15*, 19125-19128.

[120] D. M. Robinson, Y. B. Go, M. Mui, G. Gardner, Z. Zhang, D. Mastrogiovanni, E. Garfunkel, J. Li, M. Greenblatt, G. C. Dismukes, *J. Am. Chem. Soc.* **2013**, *135*, 3494-3501.

[121] Y. Zhao, Y. Zhang, Y. Ding, M. Chen, *Dalton Trans.* **2015**, *44*, 15628-15635.

[122] T. Zhang, W. Lin, *Chem. Soc. Rev.* **2014**, *43*, 5982-5993.

[123] S. Pintado, S. Goberna-Ferron, E. C. Escudero-Adan, J. R. Galan-Mascarós, *J. Am. Chem. Soc.* **2013**, 135, 13270-13273.

[124] X.-P. Shen, Y.-Z. Li, Y. Song, Z. Xu, G.-C. Guo, *Eur. J. Inorg. Chem.* **2007**, 1698-1702.

[125] Y. Yamada, K. Oyama, R. Gates, S. Fukuzumi, *Angew. Chem., Int. Ed.* **2015**, *54*, 5613-5617.

[126] R. D. Shannon, *Acta Crystallogr. Sect. A* **1969**, *32*, 751-767.

Entry for the Table of Contents (Please choose one layout)

Layout 1:

FOCUS REVIEW

Homogeneous and heterogeneous catalysis and mechanisms of photocatalytic oxidation of water by persulfate with $[Ru(bpy)]_3^{2+}$ are compared and discussed including the conversion from homogeneous precatalysts to heterogeneous catalysts.
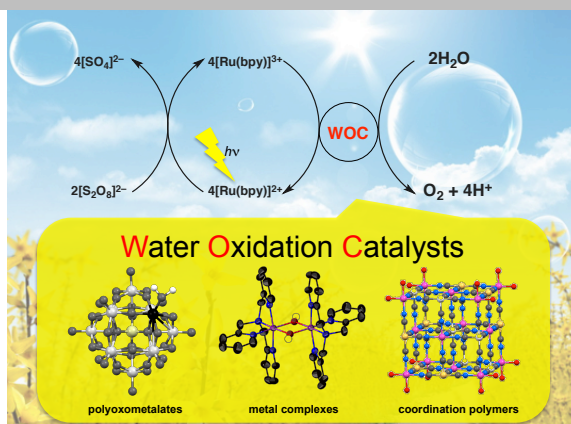
Shunichi Fukuzumi, Jieun Jung, Yusuke Yamada, Takahiko Kojima, and Wonwoo Nam

Page No. – Page No.

Homogeneous and Heterogeneous Photocatalytic Oxidation of Water by Persulfate

Layout 2:

FOCUS REVIEW

((Insert TOC Graphic here))

Author(s), Corresponding Author(s)*

Page No. – Page No.

Title

Text for Table of Contents